iScience

CellPress

Article

Genetically Engineered Flagella Form Collagen-like Ordered Structures for Inducing Stem Cell Differentiation

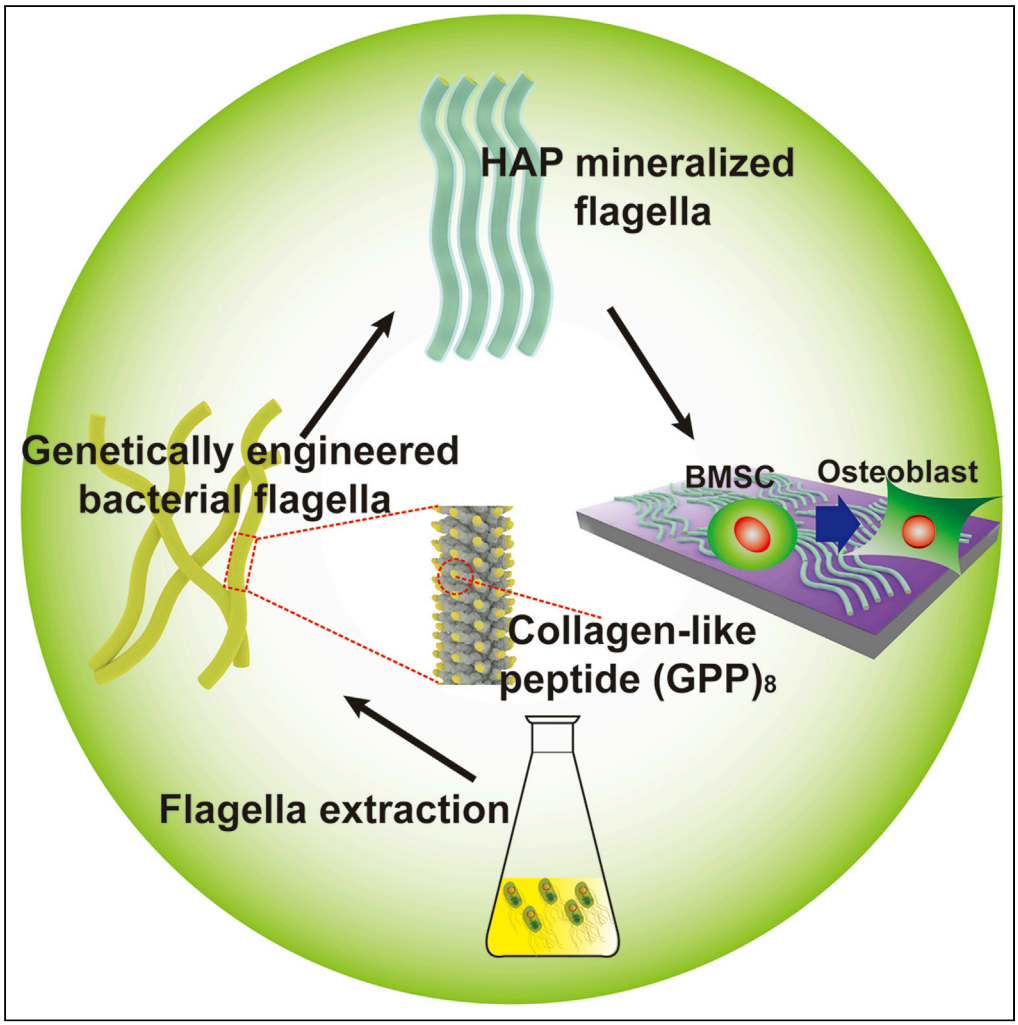

Dong Li, Ye Zhu, Tao Yang, Mingying Yang, Chuanbin Mao

cbmao@ou.edu

HIGHLIGHTS

Flagella as genetically modifiable protein nanofibers for bacterial swimming

Genetically engineering the flagella to surface display collagen-like peptides

Assembly and mineralization of flagella into mineralized collagen-like structures

Osteogenic differentiation of stem cells induced by mineralized collagen-like matrix

Li et al., iScience 17, 277–287
July 26, 2019
https://doi.org/10.1016/j.isci.2019.06.036

iScience

CellPress

Article

Genetically Engineered Flagella Form Collagen-like Ordered Structures for Inducing Stem Cell Differentiation

Dong Li,[1] Ye Zhu,[1] Tao Yang,[2] Mingying Yang,[3] and Chuanbin Mao[1,4,*]

SUMMARY

Bacteria use flagella, the protein nanofibers on their surface, as a molecular machine to swim. Flagella are polymerized from monomers, flagellins, which can display a peptide by genetic means. However, flagella as genetically modifiable nanofibers have not been used in building bone extracellular matrix-like structures for inducing stem cell differentiation in non-osteogenic medium. Here we discovered that interactions between Ca^{2+} ions and flagella (displaying a collagen-like peptide $(GPP)_8$ on every flagellin) resulted in ordered bundle-like structures, which were further mineralized with hydroxyapatite to form ordered fibrous matrix. The resultant matrix significantly induced the osteogenic differentiation of stem cells, much more efficiently than wild-type flagella and type I collagen. This work shows that flagella can be used as protein building blocks in generating biomimetic materials.

INTRODUCTION

Nature is a school for material design by creating various sophisticated materials with delicate structures and spectacular properties (Siefert et al., 2019; Chen et al., 2018; Mao et al., 2016). Many biological materials exhibit hierarchical self-assembly properties and bear well-defined patterns and organizations such as bone, tendon, seashells, and chitin (Sanchez et al., 2005; Brennan et al., 2017; Gantenbein et al., 2018; Rauner et al., 2017; Liebi et al., 2015). The extracellular matrix (ECM) of bone is a particularly hierarchical example because it is assembled from type I collagen (COL I) and hydroxyapatite (HAP). At the nanoscopic scale, the collagen molecules form fibrils by self-assembly, within which HAP nanocrystals grow with *c*-axis preferred orientation along the fibrils (Glimcher and Krane, 1968). The hierarchically organized structures of bone from the nano- to microscale are critical for its resilience, strength, stiffness, and toughness (Meyers et al., 2008). ECM mimics are known to accommodate the proliferation and differentiation of cells such as stem cells needed for tissue regeneration (Zhao et al., 2019; Chen et al., 2012; Geckil et al., 2010). Hence, various fabrication approaches have been developed to promote the self-assembly of bio-inspired materials into mimics of natural ECM in bone, including liquid crystalline assembly (Dierking, 2015; Lee et al., 2002; van t'Hag et al., 2017), electrospinning (Lee and Belcher, 2004; Alamein et al., 2013), capillary forces (Lin et al., 2010; Zhang et al., 2018), foreign molecule-induced assembly (Cao et al., 2011; Borowko et al., 2017), competitive electrostatic interactions (Yoo et al., 2006; Mendes et al., 2017), and external force-assisted assembly (Chung et al., 2011; Tkacz et al., 2014). However, it is still challenging to fabricate such materials, even mimicking the lowest level of hierarchical organization, such as the lateral parallel ordered assembly of HAP/protein nanofibers in bone.

One feasible approach to bone-inspired materials is to use bionanofibers morphologically mimicking collagen fibrils (Cao and Mao, 2007; Zhu et al., 2011; Kaur et al., 2010; Zhang et al., 2010; Wang et al., 2014; Lauria et al., 2017; Farokhi et al., 2018; Sunderland et al., 2017). Bacterial flagella are protein nanofibers naturally protruding from the bacterial cell body. As molecular machines, their movement facilitated the swimming of the bacteria in liquid. Owing to their linear ordered nanostructures and ability to be genetically engineered to display multiple peptide motifs, flagella can be potentially employed as units for the fabrication of bone-like ECM (Scheme 1). Moreover, flagellins (*FliC*s), the monomers of flagella, have been used *in vivo* as a nontoxic drug (Burdelya et al., 2008). Bacterial flagellum is a helical nanofiber self-assembled from *FliC*s with some other minor proteins at the distal ends. It contains 11 subunits (*FliC*s) per two turns. It is about 14 nm wide and 10–15 μm long (Scheme 1A). The *FliC* is a globular protein with an overall shape resembling a capitalized Greek gamma (Γ), with the upper right corner (D2 and D3 domains) pointing outward and genetically modifiable to display foreign peptides. The lower left corner of the Greek gamma is made of the N- and C-terminal domains, termed D0 and D1, of *FliC*, and binds together through non-covalent interactions and faces the center of the flagella. The solvent-exposed central region (D2 and

[1]Department of Chemistry and Biochemistry, Stephenson Life Sciences Research Center, Institute for Biomedical Engineering, Science and Technology, University of Oklahoma, Norman, OK 73072, USA

[2]School of Materials Science and Engineering, Zhejiang University, Hangzhou 310027, China

[3]Institute of Applied Bioresource Research, College of Animal Science, Zhejiang University, Yuhangtang Road 866, Hangzhou 310058, China

[4]Lead Contact

*Correspondence: cbmao@ou.edu

https://doi.org/10.1016/j.isci.2019.06.036

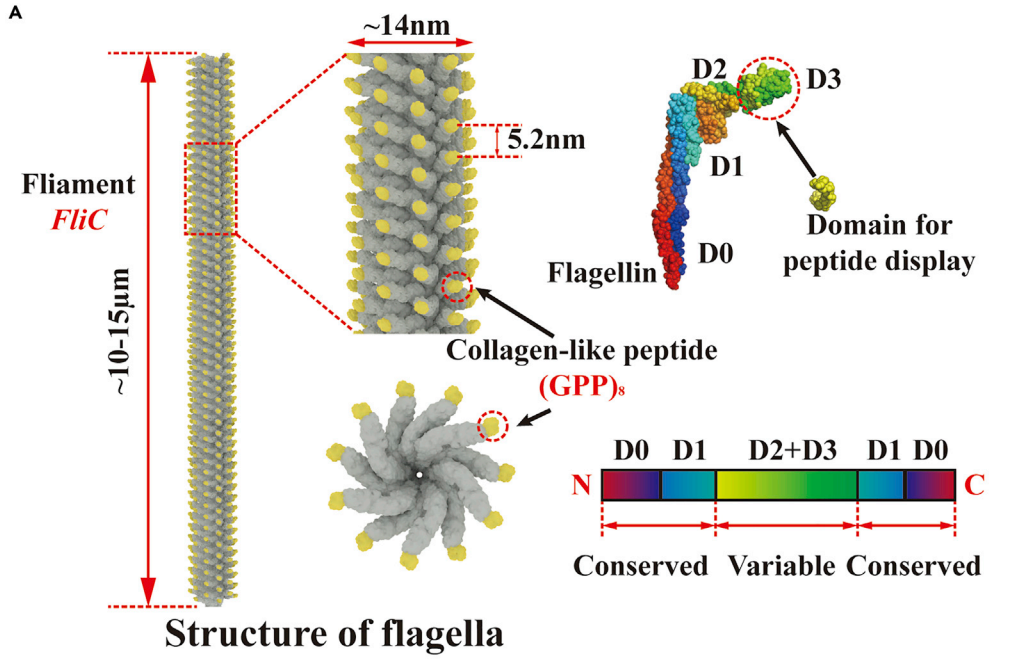

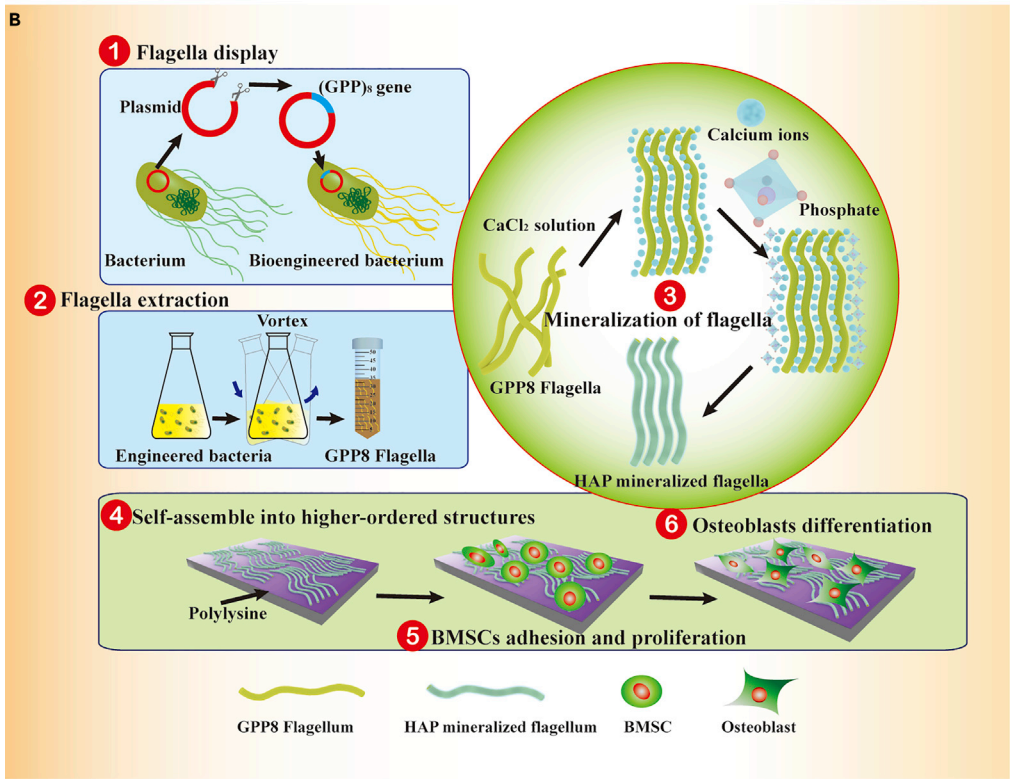

Scheme 1. Display of a Collagen-like Peptide $(GPP)_8$ on Flagella, Biomimetic Assembly and Mineralization of the Resultant GPP8 Flagella, and BMSCs' Differentiation on the GPP8 Flagella Film

(A) Schematic of a flagellum. It is mainly composed of about 30,000 flagellin (FliC) subunits. It contains 11 subunits per 2 turns. The N and C termini of flagellin (D0 and D1) are highly conserved and face the center of the filament. However, the central D2 and D3 regions are hypervariable and can be genetically engineered to display $(GPP)_8$.

Scheme 1. *Continued*

(B) Schematic of the production and self-assembly of HAP-mineralized flagellar filaments into a matrix, a closed-packed monolayer of mineralized flagella, which can support the adhesion, proliferation, and early osteogenic differentiation of BMSCs. After the peptide is displayed on the flagella by genetically engineering the bacteria (1), the flagella are purified from the surface of bacteria by vortexing (2). Then the flagella are first allowed to interact with Ca^{2+} ions and then with an HAP precursor solution to initiate the self-assembly and mineralization of the flagella (3). The resultant mineralized flagella bundles are deposited onto a polylysine-coated glass slide to form a matrix (4) to induce osteogenic differentiation of BMSCs (5 and 6).

D3 domains) of *FliC* can be modified through insertion of amino acid sequences, a technique called *flagella display* (Westerlund-Wikstrom, 2000). Each *FliC* can display a copy of foreign peptide, resulting in a distance (along the long axis) of about 2.6 nm between the neighboring *FliC* subunits (Namba et al., 1989) and generating a nanofiber with homogeneous peptide display under precise control (Scheme 1A).

Inspired by these excellent properties of the flagella, a kind of natural protein nanofiber morphologically mimicking collagen fibrils, here we genetically displayed a collagen-like peptide on the surface of flagella by genetic engineering (Scheme 1). The flagella are naturally protruding from bacterial cell body to assist cell swimming. We first detached flagella from the bacteria by vortexing. We then demonstrated formation of an inorganic-organic supramolecular nanocomposite with long-range-ordered architectures mimicking some aspects of bone ECM, by the self-assembly and mineralization of flagella. Briefly, we first allowed Ca^{2+} ions to interact with flagella to form ordered bundles. We then allowed the bundles to be incubated in an HAP precursor solution to induce HAP mineralization within the flagella bundles. The Ca^{2+} ions serve as both an inducer for the lateral assembly of the flagella into bundles and a precursor for HAP. The resultant ordered flagella structures were found to significantly induce osteogenic differentiation of bone marrow-derived stem cells (BMSCs) in a non-osteogenic basal medium.

RESULTS AND DISCUSSION

Collagens bear a repeating triplet sequence of Gly-X-Y with X position often being Pro and Y often being hydroxylated Pro. Such triplets are the key to the triple helical conformation of collagens. Therefore, $(Gly\text{-}Pro\text{-}Pro)_n$ or simply GPP_n is often considered collagen-like peptide (Fan et al., 2008). Thus we first genetically displayed a collagen-like peptide, $(Gly\text{-}Pro\text{-}Pro)_8$ (termed GPP8), on the solvent-exposed domain of every copy of *FliC* monomer constituting the flagella, leading to the production of flagella nanofibers with GPP8 fully presented on the side walls (Scheme 1). We incubated the resultant GPP8 flagella in a $CaCl_2$ solution (1–4 mM) and found that such pretreatment favored the assembly of flagella into bundles, with 2 mM $CaCl_2$ producing the most lengthy bundles (Figures S1 and S2). When the concentration of $CaCl_2$ solution was higher (10 or 20 mM), the flagella were depolymerized into subunits. Thus we chose to use 2 mM $CaCl_2$ solution to pretreat the flagella to form Ca^{2+}-decorated flagella bundles. Then the flagella bundles were purified and incubated in a 4 mM HAP-supersaturated solution for 6 days to form HAP-mineralized higher-ordered nanostructures (Figure 1). Without pretreatment and mineralization, GPP8 flagella formed a randomly stacked layer with the constituent nanofibers showing characteristic sinusoidal wave pattern in water (Figures 1A and 1C). During the pretreatment, spontaneous self-assembly of flagella nanofibers occurred (Figures S1A and S1B), promoting the formation of mineralized parallel bundles after incubation in HAP-supersaturated solution (Figures 1B and 1D). At the same time, a layer of inorganic mineral can be visualized on the flagella (Figures 1B and 1D). Selected area electron diffraction (SAED) analysis verified that the mineral was HAP owing to the presence of characteristic (211), (002), and (004) planes. It should be noted that the flagella are invisible under transmission electron microscopy without staining but their morphology can be visualized once coated with HAP. Indeed, without pretreatment with calcium ions in the absence of other ions in an HAP-supersaturated solution (Li et al., 2012), flagella displaying a collagen-like peptide cannot self-assemble into ECM mimics with collagen-like parallel-aligned matrix, indicating that interaction between the flagella and calcium ions is important for the lateral assembly of flagella into ECM mimics.

We observed a concentration-dependent self-assembly and mineralization behavior by varying concentrations of flagella in the HAP-supersaturated solution after pretreatment (Figures 2 and S3). At a low concentration of flagella (~10 μg/mL), some monodisperse flagella were coated with a layer of inorganic mineral and a few flagella were assembled into bundled nanostructures (Figure 2A). At a higher concentration of flagella (~40 μg/mL), more ordered nanostructures assembled from flagella bundles were observed (Figure 2B). Finally, at an even higher concentration of flagella (~80 μg/mL), the mineralized flagella were assembled into a close-packed monolayer (Figure 2C). Owing to the formation of parallel bundles, most

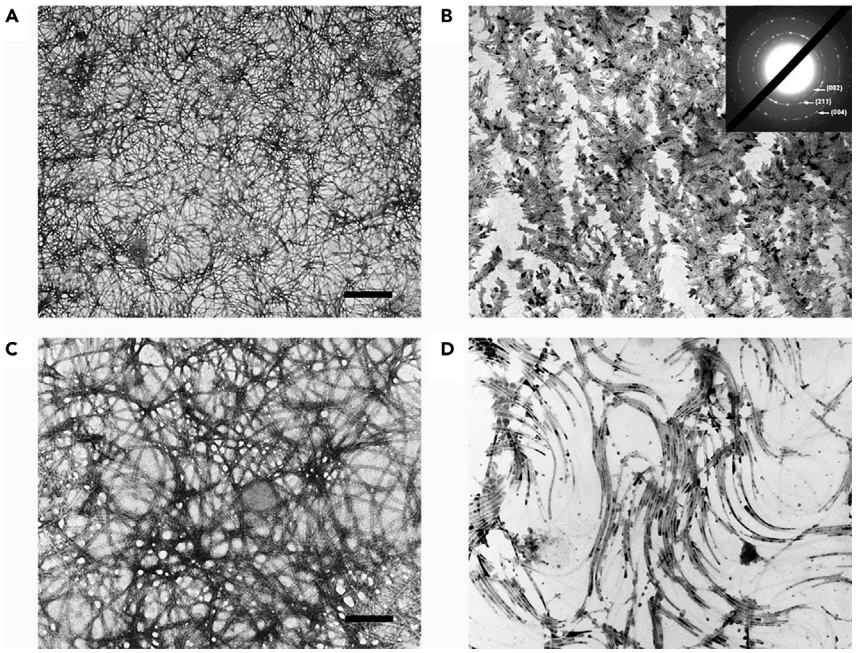

Figure 1. Transmission Electron Microscopic Images of GPP8 Flagella with or without Mineralization

(A and C) Transmission electron microscopic (TEM) images (A, low magnification; C, high magnification) of non-mineralized GPP8 flagella (due to the lack of pretreatment), showing that in water, flagella were randomly stacked and aggregated with a characteristic curly morphology. The flagella were stained with uranyl acetate. Owing to the localization of stain on the periphery of the fibers and hollow structure of flagella, tube-like filaments were observed at high magnification.

(B and D) Low (B) and high (D) magnification TEM images of flagella after pretreatment and mineralization. SAED clearly showed the characteristic (211), (002), and (004) planes of HAP (inset in B). The HAP nanocrystals located on the surface of flagella and between flagellar filaments when mineralized flagella form bundles are seen in (D). It should be noted that the TEM samples in (B) and (D) were not stained before imaging.

Scale bars, 1 μm in (A and B) and 400 nm in (C and D).

nucleated minerals were located in between neighboring filaments. The diameter of flagella is about 14 nm, and the channels between flagella filled by minerals are 25 ± 10 nm in diameter. Interestingly, the SAED pattern showed the diffraction ring for (211) plane and two pairs of diffraction arcs for (002) and (004) planes at the relatively straight segment of flagella bundles, showing the preferred crystallographic *c*-axis orientation of HAP along the flagella (Figure 2D). Energy-dispersive X-ray spectroscopy (Figure 2E) identified a Ca/P molar ratio of 1.65, similar to the theoretical ratio (1.67) in HAP [$Ca_{10}(PO_4)_6(OH)_2$]. This kind of nanostructure mimicked some key properties of bone ECM and rebuilt the structural orientation and organization between HAP and collagen fibrils in bone. The supramolecular self-assembly of GPP8 flagella was monitored by a reported turbidity assay at 320 nm (McMichael and Ou, 1979). We have found an exponential increase of absorption with the concentrations of flagella, verifying mineralized bundle formation (Figure 2F).

In a control experiment, pretreated wild-type (WT) flagella exhibited neither nucleation nor ordered assembly after mixing with 4 mM supersaturated HAP solution for 6 days. The control experiment indicated that the presence of collagen-like peptide as well as the initial interaction between Ca^{2+} ions and the peptide on the flagella drove the self-assembly and mineralization. In another control, no bundled structures were observed in the absence of Ca^{2+} ions, even though the concentration of GPP8 flagella reached up to 200 μg/mL in water without pretreatment or mineralization. These results indicated that the initial interaction between collagen-like peptides displayed on the flagellar surfaces and the Ca^{2+} ions participated in directing the organized self-assembly.

To understand the importance of the pretreatment of GPP8 flagella by Ca^{2+} ions, GPP8 flagella (80 μg/mL, 20 μL) were mixed with different concentrations of $CaCl_2$ (200 μL) (Figures S1 and S2). At a low $CaCl_2$

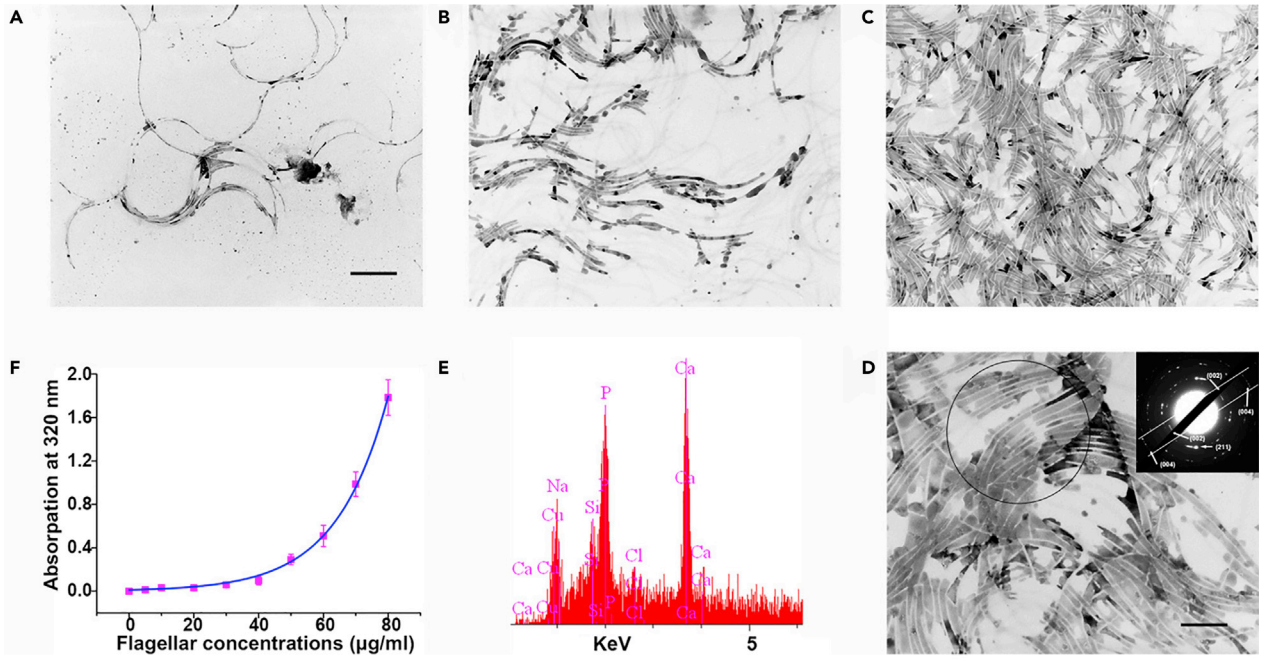
A
B
C
F
Absorpation at 320 nm
2.0
1.6
1.2
0.8
0.4
0.0
0
20
40
60
80
Flagellar concentrations (μg/ml)
E
Ca
P
Na
Cl
Si
Ca
KeV
5
D

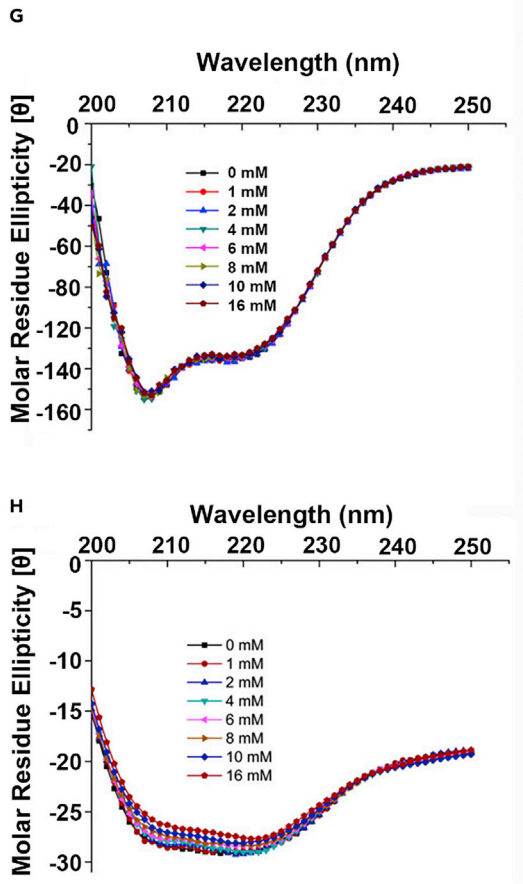
G
Wavelength (nm)
200
210
220
230
240
250
Molar Residue Ellipticity [θ]
0
-20
-40
-60
-80
-120
-140
-160
0 mM
1 mM
2 mM
4 mM
6 mM
8 mM
10 mM
16 mM
H
Wavelength (nm)
Molar Residue Ellipticity [θ]
0
-5
-10
-15
-20
-25
-30

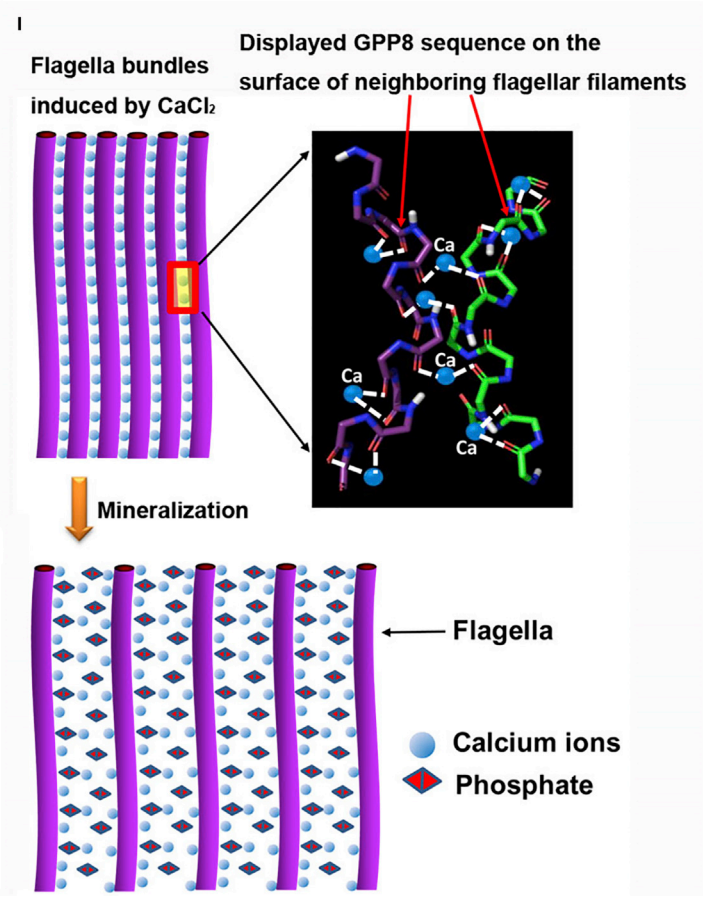
I
Flagella bundles
induced by CaCl₂
Displayed GPP8 sequence on the
surface of neighboring flagellar filaments
Ca
Mineralization
Flagella
Calcium ions
Phosphate

Figure 2. Biomimetic Self-Assembly and Mineralization of GPP8 Flagella under Different Flagella Concentrations in the HAP-Supersaturated Solution after Pretreatment with Calcium Ions

(A) Only a few bundles were formed at a low flagella concentration (~10 μg/mL).

(B) At a higher flagella concentration (~40 μg/mL), more parallel bundles were formed.

(C) A close-packed monolayer was observed when the concentration of flagella reached ~80 μg/mL.

(D) SAED pattern at the relatively straight segment of flagella bundles, showing the *c*-axis preferred orientation of HAP along the flagella (inset).

(E) Energy-dispersive X-ray spectroscopic analysis confirming a Ca/P molar ratio of 1.65. Some residues of Na and Cl came from the HAP precursor solution.

(F) An optical density measurement of flagella under different concentrations after mixing with 4 mM HAP-supersaturated solution. The solid line represents the curve-fitting result.

(G and H) A series of CD spectra of flagella under different concentrations of $CaCl_2$ (G, wild-type flagella; H, GPP8 flagella) during pretreatment.

(I) Schematic illustration of self-assembly due to interactions with Ca^{2+} ions. Ca^{2+} ions first interacted with carbonyl groups of GPP8 on flagella by chelation and induced a side-by-side aggregation. With the incorporation of phosphate ions, HAP nuclei were formed, leading to the formation of HAP on flagella. Scale bars, 400 nm in (A–C) and 250 nm in (D).

concentration (1 mM), some lateral aggregation of filaments was observed (Figure S1A). With the increase of $CaCl_2$ concentration to 4 mM, thicker parallel flagella bundles were assembled into ribbon-like structures. Moreover, the constituent nanofibers lost their characteristic curly morphology but became "straight." At the same time, some filaments were broken into shorter fragments (Figure S1B). Indeed, a high concentration of Ca^{2+} (0.5 M) could entirely depolymerize flagella (Wakabayashi et al., 1969). As expected, when the concentration of $CaCl_2$ reached 10 mM, almost all flagella were depolymerized into fragments. Surprisingly, some thicker and much more compact bundles were newly formed (Figures S1C and S2). We believe the bundles should be reassembled from the flagellar fragments or monomeric flagellins. At 20 mM $CaCl_2$, only thick and compact bundles could be observed without any flagellar fragments, implying that the flagellar fragments were totally depolymerized into monomers and then reassembled into compact bundles (Figure S1D). The formation of flagella bundles upon the increase of $CaCl_2$ concentration was also confirmed by the turbidity assay at 320 nm (Figure S4). At different concentrations of flagella (65 and 130 μg/mL), the turbidity initially increased with the concentration of $CaCl_2$ due to the formation of bundles, and then started to decrease under a higher concentration of $CaCl_2$ due to the depolymerization of flagella. It should be noted that no lateral aggregation or bundle formation occurred when a phosphate solution was mixed with GPP8 flagella.

The positively charged ions or molecules could induce the lateral aggregation of linear protein molecules (Cao et al., 2011; Wang et al., 2010). For example, the lateral packing of phage nanofibers in $CaCl_2$ was formed by the electrostatic interaction between Ca^{2+} and the negatively charged phage (Wang et al., 2010). The lateral assembly of flagella might partially arise from a similar mechanism due to the presence of large anionic surface-exposed domains (D2 and D3 from 405 to 454 amino acid positions) (Yonekura et al., 2003). On the other hand, Ca^{2+} promoted fibril formation of COL I *in vitro* by chelating with carbonyl oxygen on the COL I (Zhang et al., 2003). Circular dichroism (CD) spectroscopy and turbidity assays *in situ* also suggested that the interaction between Ca^{2+} and COL I induced the conformational change of COL I during the early phase of biomineralization (Cui et al., 2008). Molecular modeling and theoretical studies of the collagen-like peptide $(GPP)_n$ also revealed that cations were bound to carbonyl groups and the final organization of Ca^{2+} ions was similar to that in HAP crystal (Yang and Cui, 2007). The CD spectra of WT and GPP8 flagella also revealed the interactions between Ca^{2+} and GPP8 peptide on flagella (Figures 2G and 2H). The two negative peaks around 222 and 208 nm of flagella, ascribed to the perpendicular and parallel $\pi \rightarrow \pi^*$ bands of α-helix structure, respectively, were consistent with the major composition of flagellin (Yonekura et al., 2003; Kelly et al., 2005). After flagella were mixed with different concentrations of $CaCl_2$, no obvious peak changes could be observed in WT flagella (Figure 2G). However, with the increased concentrations of $CaCl_2$, the negative peak intensity was decreased in GPP8 flagella, indicating the possible conformational changes due to the interactions between the flagella and Ca^{2+} (Figure 2H).

Therefore, we propose that biomineralization of the bioengineered flagella takes place along with their lateral aggregation and ordered alignment (Figure 2I). During the pretreatment with Ca^{2+} ions, carbonyl groups on the flagella chelate Ca^{2+} ions, and when this process occurs in the neighboring filaments, a side-by-side aggregation appeared. The other polar amino acids on the flagellar surfaces might also help the lateral aggregation by the electrostatic interactions with Ca^{2+} ions, and water molecule-mediated hydrogen bonds should also facilitate the ordered alignment of the flagella (Brodsky and Ramshaw, 1997). After Ca^{2+} ions were coordinated with GPP8 flagella, phosphate ions are then electrostatically attracted

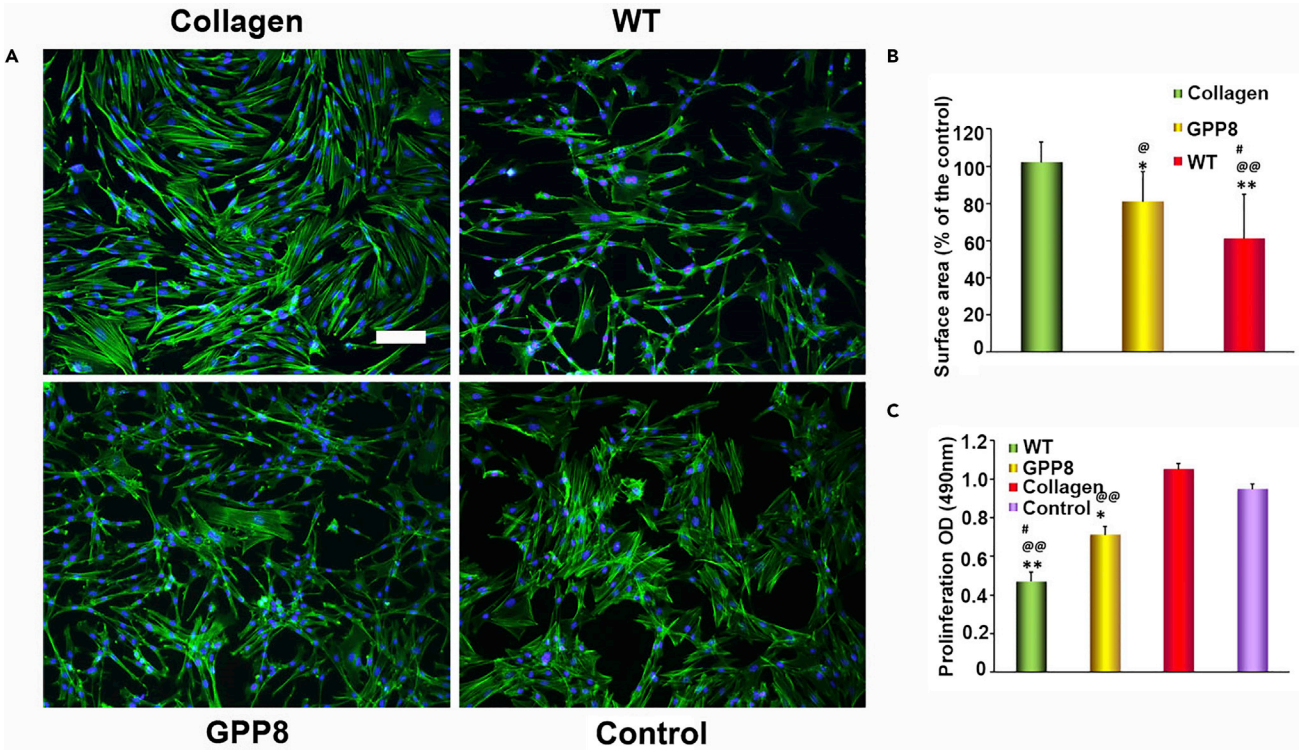

Figure 3. Fluorescence Images, Surface Spreading Area, and Proliferation of BMSCs

(A) Morphologies of BMSCs on the different substrates after 24 h. Most BMSCs exhibited a spindle-like morphology on the collagen and flagella-bearing film (WT and GPP8) but presented a well-spread morphology on polylysine (control). Scale bar, 100 μm. Cell nuclei and F-actin were marked by DAPI (blue) and fluorescein isothiocyanate-labeled phalloidin (green), respectively.

(B) Surface spreading area analysis of BMSCs.

(C) Cell proliferation on the different substrates. Collagen promoted cell proliferation, but cell proliferation on the flagella-bearing films decreased. Compared with control, *$p < 0.05$, **$p < 0.01$; compared with collagen, $^{@}p < 0.05$, $^{@@}p < 0.01$; compared with GPP8 flagella, $^{\#}p < 0.05$). Collagen, collagen-coated surface; WT, wild-type flagella-coated surface; GPP8, mineralized GPP8 flagella bundles; control, polylysine surface.

onto the nanofiber surfaces, resulting in local supersaturation with respect to HAP and the subsequent formation of HAP nuclei. More minerals are then deposited preferentially along the flagellar surface and the channels between neighboring bundled filaments (Wang et al., 2010). The proposed oriented HAP growth along flagellar surface might shed light into the HAP formation mechanism on the collagen surfaces in bone.

The biomineralized flagella bundles, which mimicked biomineralized collagen fibers, the building blocks of bone, were deposited on polylysine-functionalized substrates to form a flagella-based film (Scheme 1). Thus, BMSCs were then cultured on the film in non-osteogenic basal medium (Figures 3A and S5). The initial interactions between the cells and substrates decided cell behaviors (Kaur et al., 2010; Smith et al., 2010). BMSCs spread on the flagella-based film but not as efficiently as on the COL I or polylysine substrates. They exhibited a range of morphologies from spindle to polygonal on GPP8 flagella. Occasionally, some cells with a curly morphology were observed on the GPP8 flagella and such morphology might be induced by contact guidance response (Gerecht et al., 2007), leading to oriented growth and alignment (Figure S6). BMSCs spread much less on the WT flagella than on the other substrates, implying lack of bioactive signals on the WT flagellar surface. Scanning electron micrographs of BMSCs on collagen and flagella also revealed similar morphologies as those under light microscopy (Figure S7). Surface spreading area measurements of BMSCs further confirmed that the cells on the flagella spread significantly less than those in the control polylysine substrates (Figure 3B).

The proliferation of BMSCs was measured after 3 days (Figure 3C). The growth rate of BMSCs on the flagella substrate was lower than that on the collagen or polylysine substrate. An inverse relationship between proliferation and differentiation was usually observed in many cell types (Ettinger et al., 2011). Thus the

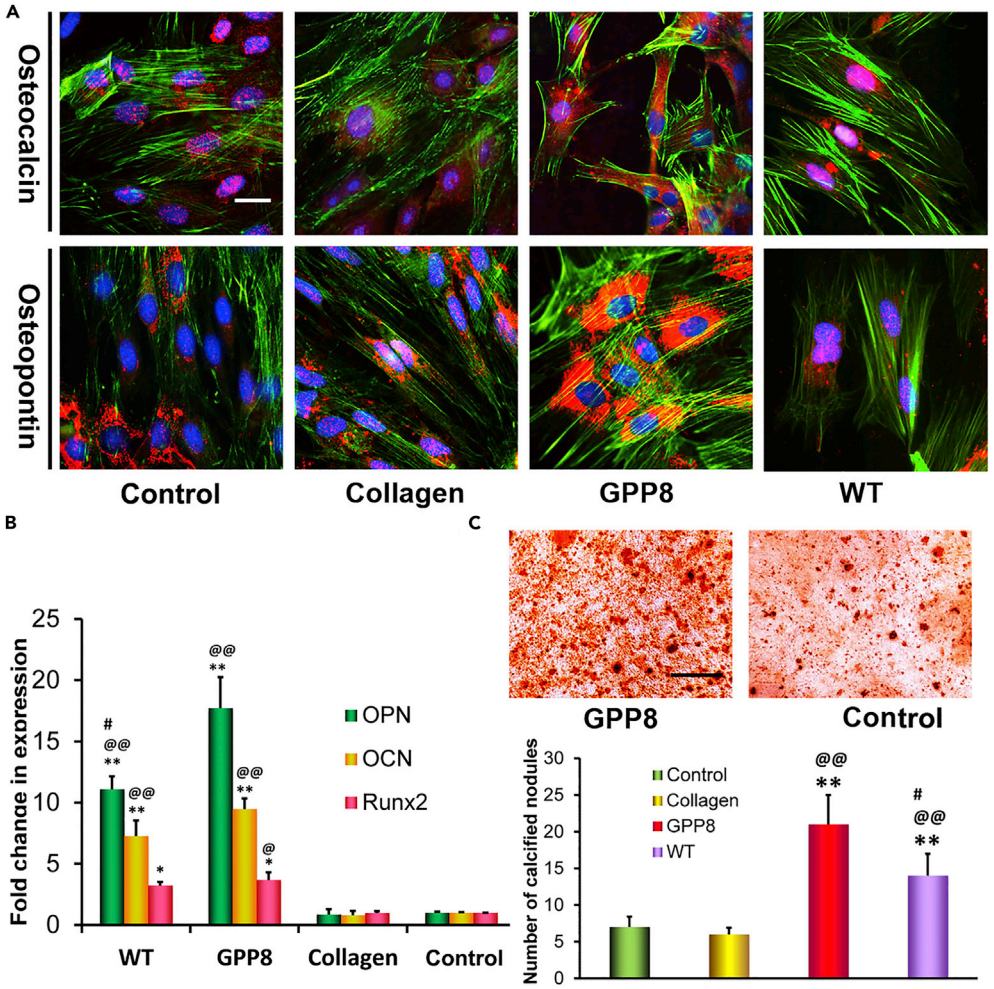

Figure 4. Differentiation of BMSCs on the Mineralized Flagella Films

(A) Immunofluorescence images showed strong expression of OPN and OCN in the cells on the mineralized self-assembled GPP8 flagella film. Collagen and polylysine also promoted the expression of OPN and OCN but at a lower level than mineralized GPP8 flagella. DAPI (blue) marked the cell nuclei, and fluorescein isothiocyanate-labeled phalloidin (green) labeled the F-actin. OPN and OCN were labeled through rhodamine-tagged antibody (red). Scale bar, 25 μm.
(B) RT-qPCR analysis showing that the flagella film could enhance mRNA expression of Runx2, OPN, and OCN. Owing to the mineralization on the GPP8 flagella film, OPN expression was significantly increased. However, gene expression between the cells on the collagen and polylysine films did not show significant difference (compared with control, $^{*}p < 0.05$, $^{**}p < 0.01$; compared with collagen, $^{@}p < 0.05$, $^{@@}p < 0.01$; compared with GPP8 flagella $^{\#}p < 0.05$).
(C) The calcium-containing minerals (calcified nodules) were stained by alizarin red S after 2 weeks. Scale bar, 400 μm. An increased number of calcified nodules indicated a higher degree of mineralization. The cells were more matured on the mineralized flagella film, indicating accelerated differentiation of BMSCs. ($^{**}p < 0.01$, versus control; $^{@@}p < 0.01$, versus collagen; $^{\#}p < 0.05$, versus GPP8 flagella). Collagen, Col I-coated surface; WT, wild-type flagella-coated surface; GPP8, mineralized GPP8 flagella bundles; control, polylysine surface.

decreased proliferation of BMSCs on the flagella-bearing substrates implied the enhancement of differentiation on the substrates.

The osteogenic differentiation of BMSCs on the biomineralized flagella films was monitored by different osteogenic markers at both protein and gene levels, and biomineralized GPP8 flagella outperformed other groups in inducing the osteogenic differentiation of BMSCs (Figure 4). Both immunofluorescence and qRT-PCR indicated higher expression levels of two osteogenesis-specific markers, osteopontin (OPN) and osteocalcin (OCN), on biomineralized GPP8 flagella than on WT flagella on day 14 (Figures 4A and 4B). Both flagella films, GPP8 and WT, showed higher expression levels of the OPN and OCN than two

control substrates (polylysine and COL I films). It was known that polylysine promoted the osteogenic differentiation of BMSCs (Galli et al., 2011). COL I was reported to enhance osteogenesis of BMSCs via ERK and Akt pathways (Tsai et al., 2010). Namely, the flagella substrates were more effective in inducing the osteogenic differentiation of BMSCs than polylysine and COL I. As a key transcription factor and early specific marker for osteogenesis, Runx2 was also up-regulated in the cells on the flagella film compared with non-flagella films (Figure 4B). After being cultured for 14 days, some cells on the GPP8 flagella film aggregated and formed calcified nodule-like structures, indicating the maturation on the osteogenic pathway (Figure S8). Quantitative analysis of alizarin red staining revealed that extracellular calcium deposits (calcified nodules) were highly increased on the flagella films compared with non-flagella films (Figure 4C). It is well known that HAP highly enhances BMSCs' differentiation toward osteoblasts (Wang et al., 2007). The nanofibrous topography can also enhance the osteogenic differentiation of stem cells (Zhu et al., 2011; Kaur et al., 2010; Smith et al., 2010). The synergistic effects of the nanotopographies of the flagella in combination with nucleated minerals and collagen-like peptide on the constituent flagella generated a microenvironment that could enhance the osteogenic differentiation of BMSCs toward osteoblasts. Thus the mineralized GPP8 flagella are more effective than non-mineralized WT flagella in inducing osteogenic differentiation, but the latter are still more effective than COL I. It should be noted that when non-collagen-like peptide is displayed on the flagella, the flagella cannot be assembled into the abundant collagen-like ordered structures seen on GPP8-displaying flagella, and consequently, the resultant flagella-based matrix can only promote the osteogenic differentiation in the osteogenic medium but cannot induce the osteogenic differentiation in the non-osteogenic basal medium (Li et al., 2019).

Compared with other display techniques such as phage display, which generally allows the display of short peptides (e.g., shorter than 20-mer) on the side wall (Zhu et al., 2011), much longer peptides (as long as a few hundred amino acids) can be tolerated on flagella without losing self-assembly properties (Westerlund-Wikström et al., 1997), making flagella capable of bearing a variety of functional peptides. Moreover, in combination with double or triple peptide display technology (Westerlund-Wikstrom, 2000), multifunctional flagella could be developed as building blocks to construct organized biomimetic scaffolds in the future. Flagella can also be easily purified in large amount with low cost and thus they are an excellent candidate for biomaterials applications. These features further allow the flagella-based ECM mimics to possess a variety of desired biological functions in regenerative medicine by genetic display of functional peptides instead of by using chemical conjugation. In addition, flagella have a Young's modulus within the range of 1–100 GPa (Flynn and Ma, 2004) whereas HAP single crystals have a Young's modulus of ~150 GPa (Zamiri and De, 2011). Thus biomineralized collagen-like flagella structures are unique soft-hard hybrid materials that may also modulate stem cell fate through their mechanical cues other than the topographical cues. Finally, flagellins, the subunits of flagella, are anti-tumor and radioprotective agents (Hajam et al., 2017). Thus flagella-based ECM mimics may hold promise for regenerating tissues while avoiding tumor growth.

In conclusion, bacterial flagella, the molecular machines for driving the bacteria to swim, were employed as natural biotemplates to form ordered structures as building blocks for fabricating bone-inspired, osteogenic materials. With collagen-like peptides displayed on the side walls, the bioengineered flagella could interact with Ca^{2+} ions to form bundles and then mineralized in an HAP precursor solution to form bone ECM-like matrix. The presence of collagen-like peptides on the flagellar surfaces as well as the Ca^{2+} ions were the two important factors that contributed to the coupled self-assembly and biomineralization. The matrix assembled from the flagella was biocompatible and could support the adhesion and growth of BMSCs. Moreover, the nanotopography and surface chemistry of the flagella-based matrix significantly induced the osteogenic differentiation of BMSCs. The biomimetic nucleation and self-assembly of the bioengineered flagella represents a novel approach to bioinspired ordered and hierarchical materials.

Limitations of the Study

Mechanical cues can also influence the fate of stem cells. Although this study shows that flagella-based mineralized collagen-like structures can induce the osteogenic differentiation of BMSCs, this study can be further improved by investigating the stiffness of the collagen-like structure. It is likely that the topographical and chemical cues presented by the collagen-like structure play a dominant role in directing the osteogenic differentiation; studying the effect of the stiffness of the collagen-like structures on osteogenic differentiation will give us a more complete picture of the flagella-directed osteogenic differentiation.

METHODS

All methods can be found in the accompanying Transparent Methods supplemental file.

SUPPLEMENTAL INFORMATION

Supplemental Information can be found online at https://doi.org/10.1016/j.isci.2019.06.036.

ACKNOWLEDGMENTS

We would like to thank the partial financial support from the Office of Basic Energy Sciences within the Department of Energy (DOE) Office of Science (DE-SC0016567). We would also like to thank Salete Newton and Philip Klebba for assisting the peptide display on flagella.

AUTHOR CONTRIBUTIONS

C.M. conceived the project. D.L. and Y.Z. performed the experiments. All authors analyzed the data. T.Y. designed the illustrations. D. L., Y.Z., M.Y., and C.M. wrote the manuscript.

DECLARATION OF INTERESTS

The authors declare no competing interests.

Received: May 3, 2019
Revised: June 13, 2019
Accepted: June 28, 2019
Published: July 26, 2019

REFERENCES

Alamein, M.A., Liu, Q., Stephens, S., Skabo, S., Warnke, F., Bourke, R., Heiner, P., and Warnke, P.H. (2013). Nanospiderwebs: artificial 3D extracellular matrix from nanofibers by novel clinical grade electrospinning for stem cell delivery. Adv. Healthc. Mater. *2*, 702–717.

Borowko, M., Rzysko, W., Sokolowski, S., and Staszewski, T. (2017). Self-assembly of Janus disks induced by small molecules in two-dimensional systems. J. Chem. Phys. *147*, 014904.

Brennan, O., Sweeney, J., O'Meara, B., Widaa, A., Bonnier, F., Byrne, H.J., O'Gorman, D.M., and O'Brien, F.J. (2017). A natural, calcium-rich marine multi-mineral complex preserves bone structure, composition and strength in an ovariectomised rat model of osteoporosis. Calcif. Tissue Int. *101*, 445–455.

Brodsky, B., and Ramshaw, J.A.M. (1997). The collagen triple-helix structure. Matrix Biol. *15*, 545–554.

Burdelya, L.G., Krivokrysenko, V.I., Tallant, T.C., Strom, E., Gleiberman, A.S., Gupta, D., Kurnasov, O.V., Fort, F.L., Osterman, A.L., DiDonato, J.A., et al. (2008). An agonist of toll-like receptor 5 has radioprotective activity in mouse and primate models. Science *320*, 226–230.

Cao, B., and Mao, C. (2007). Oriented nucleation of hydroxylapatite crystals on spider dragline silks. Langmuir *23*, 10701–10705.

Cao, B., Xu, H., and Mao, C. (2011). Controlled self-assembly of rodlike bacterial pili particles into ordered lattices. Angew. Chem. Int. Ed. *50*, 6264–6268.

Chen, N., Zhang, Z., Soontornworajit, B., Zhou, J., and Wang, Y. (2012). Cell adhesion on an artificial extracellular matrix using aptamer-functionalized PEG hydrogels. Biomaterials *33*, 1353–1362.

Chen, H.W., Ran, T., Gan, Y., Zhou, J.J., Zhang, Y., Zhang, L.W., Zhang, D.Y., and Jiang, L. (2018). Ultrafast water harvesting and transport in hierarchical microchannels. Nat. Mater. *17*, 935–942.

Chung, W.-J., Oh, J.-W., Kwak, K., Lee, B.Y., Meyer, J., Wang, E., Hexemer, A., and Lee, S.-W. (2011). Biomimetic self-templating supramolecular structures. Nature *478*, 364–368.

Cui, F.Z., Wang, Y., Cai, Q., and Zhang, W. (2008). Conformation change of collagen during the initial stage of biomineralization of calcium phosphate. J. Mater. Chem. *18*, 3835–3840.

Dierking, I. (2015). Liquid crystals: materials design and self-assembly. Liq. Cryst. Today *24*, 116–118.

Ettinger, A.W., Wilsch-Brauninger, M., Marzesco, A.-M., Bickle, M., Lohmann, A., Maliga, Z., Karbanova, J., Corbeil, D., Hyman, A.A., and Huttner, W.B. (2011). Proliferating versus differentiating stem and cancer cells exhibit distinct midbody-release behaviour. Nat. Commun. *2*, 503.

Fan, C.Y., Huang, C.C., Chiu, W.C., Lai, C.C., Liou, G.G., Li, H.C., and Chou, M.Y. (2008). Production of multivalent protein binders using a self-trimerizing collagen-like peptide scaffold. FASEB J. *22*, 3795–3804.

Farokhi, M., Mottaghitalab, F., Samani, S., Shokrgozar, M.A., Kundu, S.C., Reis, R.L., Fatahi, Y., and Kaplan, D.L. (2018). Silk fibroin/hydroxyapatite composites for bone tissue engineering. Biotechnol. Adv. *36*, 68–91.

Flynn, T.C., and Ma, J.P. (2004). Theoretical analysis of twist bend ratio and mechanical moduli of bacterial flagellar hook and filament. Biophys. J. *86*, 3204–3210.

Galli, D., Benedetti, L., Bongio, M., Maliardi, V., Silvani, G., Ceccarelli, G., Ronzoni, F., Conte, S., Benazzo, F., Graziano, A., et al. (2011). In vitro osteoblastic differentiation of human mesenchymal stem cells and human dental pulp stem cells on poly-L-lysine-treated titanium-6-aluminium-4-vanadium. J. Biomed. Mater. Res. A *97A*, 118–126.

Gantenbein, S., Masania, K., Woigk, W., Sesseg, J.P.W., Tervoort, T.A., and Studart, A.R. (2018). Three-dimensional printing of hierarchical liquid-crystal-polymer structures. Nature *561*, 226–230.

Geckil, H., Xu, F., Zhang, X., Moon, S., and Demirci, U. (2010). Engineering hydrogels as extracellular matrix mimics. Nanomed *5*, 469–484.

Gerecht, S., Bettinger, C.J., Zhang, Z., Borenstein, J.T., Vunjak-Novakovic, G., and Langer, R. (2007). The effect of actin disrupting agents on contact guidance of human embryonic stem cells. Biomaterials *28*, 4068–4077.

Glimcher, M.J., and Krane, S.M. (1968). Organization and structure of bone, and the mechanism of calcification. Treatise Collagen *2*, 67–251.

Hajam, I.A., Dar, P.A., Shahnawaz, I., Jaume, J.C., and Lee, J.H. (2017). Bacterial flagellin-a potent immunomodulatory agent. Exp. Mol. Med. *49*, e373.

Kaur, G., Valarmathi, M.T., Potts, J.D., Jabbari, E., Sabo-Attwood, T., and Wang, Q. (2010). Regulation of osteogenic differentiation of rat

bone marrow stromal cells on 2D nanorod substrates. Biomaterials *31*, 1732–1741.

Kelly, S.M., Jess, T.J., and Price, N.C. (2005). How to study proteins by circular dichroism. Biochim. Biophys. Acta *1751*, 119–139.

Lauria, I., Dickmeis, C., Roder, J., Beckers, M., Rutten, S., Lin, Y.Y., Commandeur, U., and Fischer, H. (2017). Engineered Potato virus X nanoparticles support hydroxyapatite nucleation for improved bone tissue replacement. Acta Biomater. *62*, 317–327.

Lee, S.-W., and Belcher, A.M. (2004). Virus-based fabrication of micro- and nanofibers using electrospinning. Nano Lett. *4*, 387–390.

Lee, S.-W., Mao, C., Flynn, C.E., and Belcher, A.M. (2002). Ordering of quantum dots using genetically engineered viruses. Science *296*, 892–895.

Li, D., Newton, S.M., Klebba, P.E., and Mao, C. (2012). Flagellar display of bone-protein-derived peptides for studying peptide-mediated biomineralization. Langmuir *28*, 16338–16346.

Li, D., Zhu, Y., Yang, T., Yang, M., and Mao, C. (2019). Bacterial flagella as an osteogenic differentiation nano-promoter. Nanoscale Horiz. https://doi.org/10.1039/c9nh00124g.

Liebi, M., Georgiadis, M., Menzel, A., Schneider, P., Kohlbrecher, J., Bunk, O., and Guizar-Sicairos, M. (2015). Nanostructure surveys of macroscopic specimens by small-angle scattering tensor tomography. Nature *527*, 349–352.

Lin, Y., Balizan, E., Lee, L.A., Niu, Z., and Wang, Q. (2010). Self-assembly of rodlike bio-nanoparticles in capillary tubes. Angew. Chem. Int. Ed. *49*, 868–872.

Mao, L.B., Gao, H.L., Yao, H.B., Liu, L., Colfen, H., Liu, G., Chen, S.M., Li, S.K., Yan, Y.X., Liu, Y.Y., and Yu, S.H. (2016). Synthetic nacre by predesigned matrix-directed mineralization. Science *354*, 107–110.

McMichael, J.C., and Ou, J.T. (1979). Binding of lysozyme to common pili of Escherichia coli. J. Bacteriol. *138*, 976–983.

Mendes, A.C., Strohmenger, T., Goycoolea, F., and Chronakis, I.S. (2017). Electrostatic self-assembly of polysaccharides into nanofibers. Colloids Surf. A *531*, 182–188.

Meyers, M.A., Chen, P.-Y., Lin, A.Y.-M., and Seki, Y. (2008). Biological materials: structure and mechanical properties. Prog. Mater. Sci. *53*, 1–206.

Namba, K., Yamashita, I., and Vonderviszt, F. (1989). Structure of the core and central channel of bacterial flagella. Nature *342*, 648–654.

Rauner, N., Meuris, M., Zoric, M., and Tiller, J.C. (2017). Enzymatic mineralization generates ultrastiff and tough hydrogels with tunable mechanics. Nature *543*, 407–410.

Sanchez, C., Arribart, H., and Giraud Guille, M.M. (2005). Biomimetism and bioinspiration as tools for the design of innovative materials and systems. Nat. Mater. *4*, 277–288.

Siefert, E., Reyssat, E., Bico, J., and Roman, B. (2019). Bio-inspired pneumatic shape-morphing elastomers. Nat. Mater. *18*, 24–28.

Smith, L.A., Liu, X.H., Hu, J.A., and Ma, P.X. (2010). The Enhancement of human embryonic stem cell osteogenic differentiation with nano-fibrous scaffolding. Biomaterials *31*, 5526–5535.

Sunderland, K.S., Yang, M.Y., and Mao, C.B. (2017). Phage-enabled nanomedicine: from probes to therapeutics in precision medicine. Angew. Chem. Int. Ed. *56*, 1964–1992.

Tkacz, R., Oldenbourg, R., Fulcher, A., Miansari, M., and Majumder, M. (2014). Capillary-force-assisted self-assembly (CAS) of highly ordered and anisotropic graphene-based thin films. J. Phys. Chem. C *118*, 259–267.

Tsai, K.-S., Kao, S.-Y., Wang, C.-Y., Wang, Y.-J., Wang, J.-P., and Hung, S.-C. (2010). Type I collagen promotes proliferation and osteogenesis of human mesenchymal stem cells via activation of ERK and Akt pathways. J. Biomed. Mater. Res. A *94A*, 673–682.

van t'Hag, L., Gras, S.L., Conn, C.E., and Drummond, C.J. (2017). Lyotropic liquid crystal engineering moving beyond binary compositional space - ordered nanostructured amphiphile self-assembly materials by design. Chem. Soc. Rev. *46*, 2705–2731.

Wakabayashi, K., Hotani, H., and Asakura, S. (1969). Polymerization of salmonella flagellin in the presence of high concentrations of salts. Biochim. Biophys. Acta *175*, 195–203.

Wang, H., Li, Y., Zuo, Y., Li, J., Ma, S., and Cheng, L. (2007). Biocompatibility and osteogenesis of biomimetic nano-hydroxyapatite/polyamide composite scaffolds for bone tissue engineering. Biomaterials *28*, 3338–3348.

Wang, F., Cao, B., and Mao, C. (2010). Bacteriophage bundles with prealigned Ca^{2+} initiate the oriented nucleation and growth of hydroxylapatite. Chem. Mater. *22*, 3630–3636.

Wang, J.L., Yang, M.Y., Zhu, Y., Wang, L., Tomsia, A.P., and Mao, C.B. (2014). Phage nanofibers induce vascularized osteogenesis in 3D printed bone scaffolds. Adv. Mater. *26*, 4961–4966.

Westerlund-Wikstrom, B. (2000). Peptide display on bacterial flagella: principles and applications. Int. J. Med. Microbiol. *290*, 223–230.

Westerlund-Wikström, B., Tanskanen, J., Virkola, R., Hacker, J., Lindberg, M., Skurnik, M., and Korhonen, T.K. (1997). Functional expression of adhesive peptides as fusions to Escherichia coli flagellin. Protein Eng. *10*, 1319–1326.

Yang, B., and Cui, F.Z. (2007). Molecular modeling and mechanics studies on the initial stage of the collagen-mineralization process. Curr. Appl. Phys. *7*, e2–e5.

Yonekura, K., Maki-Yonekura, S., and Namba, K. (2003). Complete atomic model of the bacterial flagellar filament by electron cryomicroscopy. Nature *424*, 643–650.

Yoo, P.J., Nam, K.T., Qi, J., Lee, S.-K., Park, J., Belcher, A.M., and Hammond, P.T. (2006). Spontaneous assembly of viruses on multilayered polymer surfaces. Nat. Mater. *5*, 234–240.

Zamiri, A., and De, S. (2011). Mechanical properties of hydroxyapatite single crystals from nanoindentation data. J. Mech. Behav. Biomed. Mater. *4*, 146–152.

Zhang, W., Huang, Z.-L., Liao, S.-S., and Cui, F.-Z. (2003). Nucleation sites of calcium phosphate crystals during collagen mineralization. J. Am. Ceram. Soc. *86*, 1052–1054.

Zhang, Y., Wu, C., Friis, T., and Xiao, Y. (2010). The osteogenic properties of CaP/silk composite scaffolds. Biomaterials *31*, 2848–2856.

Zhang, C.Q., Adler, P.H., Monaenkova, D., Andrukh, T., Pometto, S., Beard, C.E., and Kornev, K.G. (2018). Self-assembly of the butterfly proboscis: the role of capillary forces. J. R. Soc. Interface *15*, 20180229.

Zhao, N., Coyne, J., Xu, M., Zhang, X., Suzuki, A., Shi, P., Lai, J., Fong, G.-H., Xiong, N., and Wang, Y. (2019). Assembly of bifunctional aptamer–fibrinogen macromer for VEGF delivery and skin wound healing. Chem. Mater. *31*, 1006–1015.

Zhu, H., Cao, B., Zhen, Z., Laxmi, A.A., Li, D., Liu, S., and Mao, C. (2011). Controlled growth and differentiation of MSCs on grooved films assembled from monodisperse biological nanofibers with genetically tunable surface chemistries. Biomaterials *32*, 4744–4752.

ISCI, Volume *17*

Supplemental Information

Genetically Engineered Flagella Form Collagen-like Ordered Structures for Inducing Stem Cell Differentiation

Dong Li, Ye Zhu, Tao Yang, Mingying Yang, and Chuanbin Mao

Supplemental Information

Genetically engineered flagella form collagen-like ordered structures for inducing stem cell differentiation

Dong Li, Ye Zhu, Tao Yang, Mingying Yang, and Chuanbin Mao

Transparent Methods

Flagella display. The bioengineered flagella were constructed using recombinant DNA methods. $(GPP)_8$ peptide was displayed at the exposed domain of the flagellin. Specifically, DNA primers encoding 8 continuous GPP sequences were synthesized. N-terminal and C-terminal of the primers contained the sequences of restriction enzyme sites XhoI and BglII, respectively. The forward and reverse single-stranded DNA were annealed into a double-stranded DNA by cooling slowly in the boiling water. The DNA with oriented sticky ends was cloned into a plasmid with XhoI and BglII restriction enzyme cloning sites. A Salmonella strain with flagellin gene knocked out was then transformed by the plasmid. Before transformation, this strain could not swim and lose motility in the semisolid medium due to the lack of flagellin expression. After the transformation, the positive clone with Amp resistance and the highest motility was selected and confirmed by DNA sequencing. The positive clone was then inoculated into a small volume (5 mL) of LB-Amp (0.1%) and incubated overnight at 37℃ with shaking (250 rpm). Then, the cultured media (1 mL) was transferred into 1 L of LB-Amp (0.1%) and continued to be incubated under the same conditions.

Flagella purification. The bioengineered bacterial flagella were purified from the surface of bacteria via vigorously vortexing for 90 s. The resultant supernatant contained the detached flagella. Through the ultracentrifugation of the supernatant at 12,000 g for 20 min, the flagella were purified and re-dissolved in ddH_2O.

Self-assembly of mineralization of flagella. To prepare HAP-supersaturated solution (4 mM), first HAP powder with a calcium/phosphate molar ratio of 1.67 was dissolved in 100 mM HCl solution to prepare a stock solution. KOH (0.05 M) was used to adjust the pH value of the solution to 7.0. NaCl was placed into the stock solution until its concentration became 200 mM. Finally, distilled water was added to the resultant solution to make the concentration of Ca^{2+} reach 4 mM. 20 μl of flagella solution was mixed with 2 mM $CaCl_2$ solution (200 μl). Then the resultant flagella bundles were purified by centrifugation and suspended in HAP-supersaturated solution to induce the mineralization of flagella. After 6 days, a drop of aqueous solution was placed on the carbon TEM grid. The TEM grid was cleaned with ddH_2O and dried in air. The specimens were then imaged under TEM at 80 kV.

Turbidity measurements. The flagella solutions were placed into a 2 mm cell. The cell was closed to prevent evaporation. Optical density of the flagella solutions at 320 nm, reflecting the turbidity, was monitored at different time points by a nano-spectrophotometer.

Circular Dichroism (CD) spectroscopic measurements. CD spectra were measured using a circular dichrometer under a spectral band width of 1 nm. A total of 300 μl of bioengineered flagellar solution (1 mg/ml) was placed in a 0.1 cm cell. The resultant CD spectra were graphed as

[θ] in units of deg 10^{-3} cm^2 $dmol^{-1}$. Three measurements from the same sample were averaged to obtain a spectrum.

BMSCs isolation and culture: BMSCs isolated from the bone marrow of a rat (Harlan) were cultured in a growth medium made of DMEM (low glucose) supplemented with 10% FBS and 1% penicillin/streptomycin. Cells were subcultured using trypsin/EDTA and maintained at 37 ℃ in a humidified atmosphere of 5% CO_2. This animal work was approved by IACUC of the University of Oklahoma. The cell morphology was characterized by SEM.

Scanning Electron Microscopy (SEM) examination: BMSCs were seeded on scaffolds made of mineralized flagella or collagen at a density of 1×10^4 cells/ml in a 24-well culture plate with a pre-cleaned cover-slip in each well. After the cells were cultured for 24 h, they were washed with PBS. Then 2.5% glutaraldehyde in 0.1× PBS was used to fix the cells for 1 h. The cells were washed again with PBS. Then ethanol (50%, 70%, 90%, and 100%) was used to dehydrate the cells serially with each concentration for 30 min. The samples were further dehydrated by a CO_2 supercritical point dryer. The morphology of BMSCs was observed using SEM (JEOL JSM-840). The surface area of the cells was calculated by the computer-assisted planimetry from at least 45 cells per sample in the SEM micrographs by means of the automated measurement function of Image J (downloaded from the National Institute of Health, Bethesda, MD, USA, available at http://rsb.info.nih.gov/ij/).

Proliferation assay on different substrates by Methylthiazoletetrazolium (MTT) test: BMSCs were plated on different substrates at 4×10^3 cells/well in the plates in DMEM for 72 h and

evaluated using MTT assay following manufacturer's protocol. The absorbance at 490 nm was detected by a spectrophotometric microplate reader.

Differentiation assays of BMSCs on different substrates: The osteogenic differentiation was characterized by three assays as described in detail in the following three sections, including immunofluorescence imaging of marker proteins (OCN and OPN), RT-qPCR analysis of the marker genes (OCN, OPN and Rux2), and alizarin red S staining of calcified nodules.

Immunofluorescence examination: The cells cultured in a 24-well plate with a round pre-cleaned cover-slip in each well were washed twice with PBS and fixed with ethanol (70% in PBS) for half an hour. After the samples were washed with PBST buffer (1× PBS containing 0.05% Tween-20), they were incubated with 0.1% Triton X-100 in PBS for 10 min to permeabilize the cell membranes. Afterwards, the samples were blocked in 5% BSA for 1 h. The primary antibodies (either anti-OPN (1:500, Abcam Biotechnology) or anti-OCN (1:1000, Santa Cruz Biotechnology) were diluted in 5% BSA and incubated with cells overnight at 4 °C. After 3 washes with PBST (5 minutes each), secondary antibodies of Goat anti-rabbit IgG-TRITC (1:500, Santa Cruz Biotechnology) at 1:100 dilutions in blocking buffer were added. Filamentous actin was stained with FITC-conjugated phalloidin (1:40, Invitrogen) in PBS and nuclei were stained with DAPI. The coverslips with samples were then inverted onto the glass slides and mounted. The images were collected by a Nikon fluorescence microscope.

Quantitative real-time PCR examination: The cells were harvested on day 14. Total RNA isolation with reverse transcription to cDNA was prepared with Ambion® Cells-to-cDNA™ II Kit

from Invitrogen. Power SYBR Green PCR master mix from Applied Biosystems was applied in this study for monitoring the changes of DNA during qPCR process. Quantitative examination of the samples was done by a mini Fast real-time PCR system (Bio-rad Laboratories) using 10 µl SYBR Green I mastermix, 5 µl cDNA templates, and 3 pmol/ml of each primer in a final reaction volume of 50 µl. The PCR reaction involving 45 cycles was performed with acidic ribosomal phosphoprotein P0 (Arbp) as a housekeeping gene. Agarose gel electrophoresis was conducted to confirm the specificity of the PCR amplification. The primer sequences for qPCR were:

Osteopontin (OPN):

Forward 5'-GACGGCCGAGGTGATAGCTT-3'

Reverse 5'-CATGGCTGGTCTTCCCGTTGC-3'

Osteocalcin (OCN):

Forward 5'-AAAGCCCAGCGACTCT-3'

Reverse 5'-CTAAACGGTGGTGCCATAGAT-3'

Runx2:

Forward 5'–GCTTCTCCAACCCACGAATG–3'

Reverse 5'–GAACTGATAGGACGCTGACGA–3'

Arbp (Housekeeping gene)

Forward 5' -CGACCTGGAAGTCCAACTAC–3'

Reverse 5'–ATCTGCTGCATCTGCTTG–3'.

Calcium assay: The cells were seeded at a density of 4×10^3 cells per well in 96-well plates coated with mineralized flagella samples and grown in osteogenic media for 2 weeks. The cells were fixed in 4% paraformaldehyde for 40 min and the mineralized nodules were stained using

0.1% alizarin red S at a pH value of about 4.1 for 30 min. The number of calcified nodules was counted in each well. To prevent bias, each experimental group was calculated by averaging the five counted wells.

Statistical analysis. Data was represented as mean ± standard deviation in all the figures. Student t tests were carried out to determine significant difference. Significant difference was set as p-values less than 0.05 or 0.01 in all analysis. All experiments were repeated for at least 3 times.

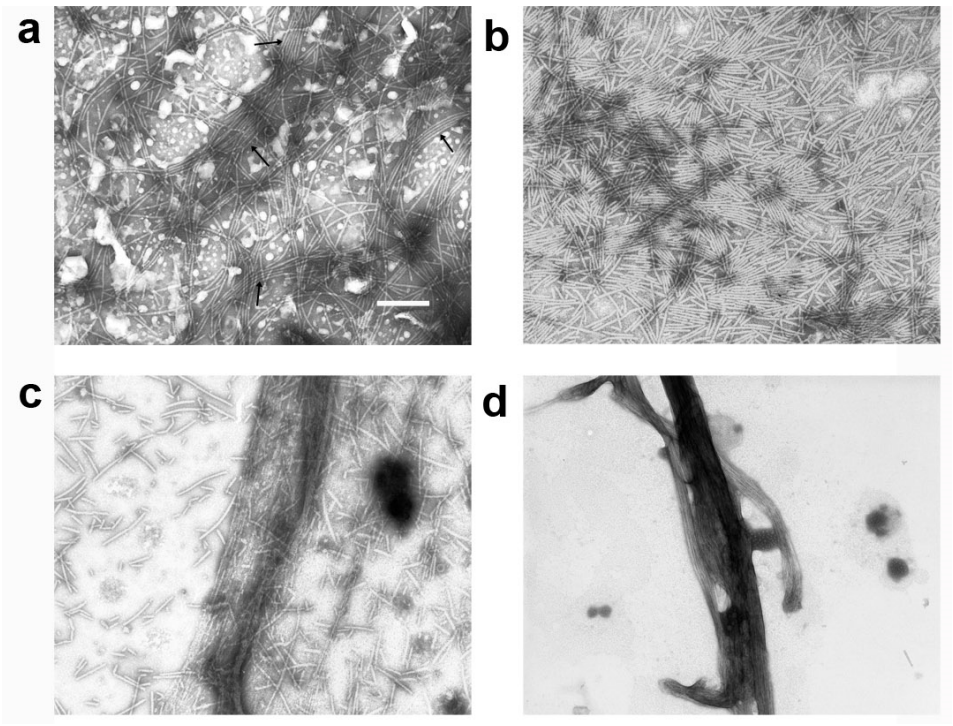

Figure S1. Representative micrographs of bioengineered flagella bundle formation induced by different concentrations of $CaCl_2$, Related to Figure 1 and 2. a, At a low concentration of $CaCl_2$ (1 mM), flagella were assembled into bundles by lateral aggregation of filaments as marked by arrows. **b,** At a higher concentration (4 mM), ribbon-like nanostructures were formed by parallel flagella bundles. Relatively "straight" filaments were observed due to the breaking of long filaments. **c,** At 10 mM of $CaCl_2$, flagella were broken into short fragments and formed thick and compact bundles. **d,** When $CaCl_2$ reached 20 mM, all depolymerized flagella were repolymerized into compact bundles. (Scale bar: 400 nm).

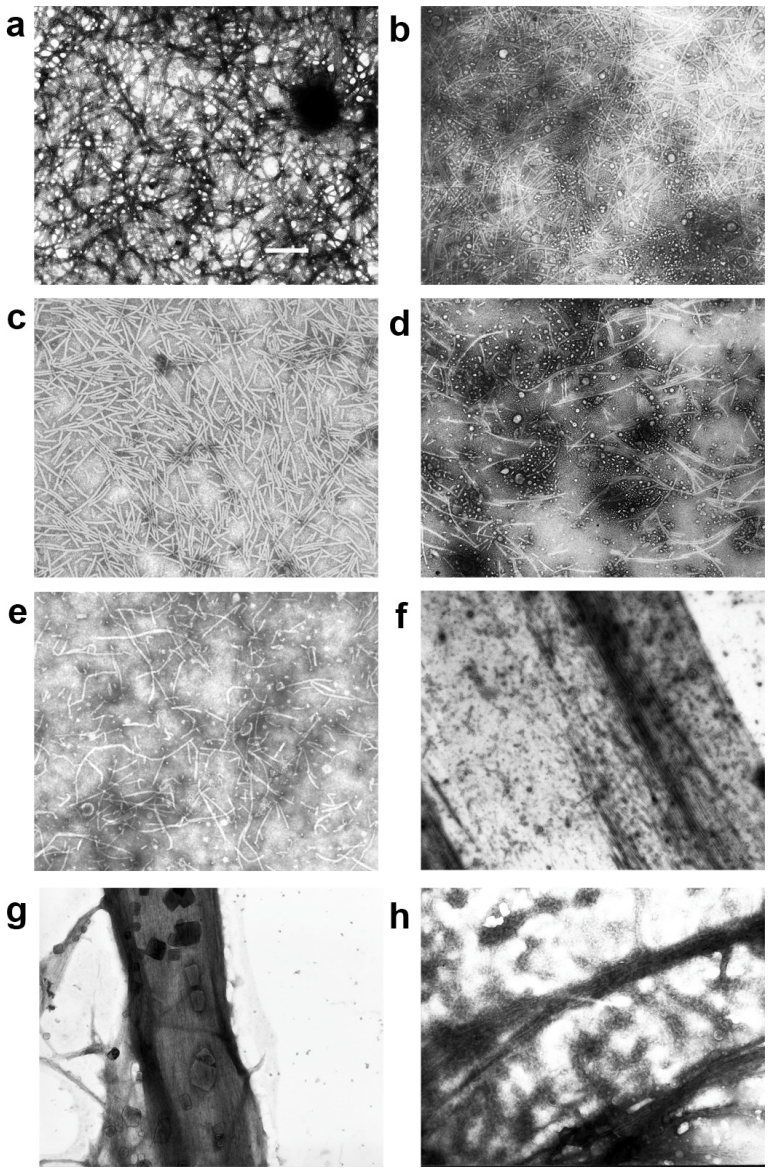

Figure S2. More TEM micrographs of flagella under different concentrations of $CaCl_2$, Related to Figure 1 and 2. a, At a concentration of $CaCl_2$ (2 mM), close-packed and ribbon-like parallel flagella bundles were observed. **b,** At 3 mM of $CaCl_2$, the ribbon-like bundles became more compact. **c,** At a higher concentration (6 mM) of $CaCl_2$, all flagella were broken into short fragments and most fragments formed parallel nanostructures. **d,** At 8 mM of $CaCl_2$, more flagella were broken into small fragments and some of them were depolymerized. **e,** When $CaCl_2$ reached 10 mM, the short flagella were randomly packed and lost their original sinusoidal wave

morphology. **f,** At some areas, very large ribbon-like structures could be observed. **g,** All flagella were disappeared and only large ribbon-like structures could be observed at 20 mM of $CaCl_2$. **h,** The linear structures inside the ribbon-like structures suggested that they might be re-assembled from small fragments of flagella or monomeric flagellins (Scale bar: 400 nm).SEM topographies of polylysine coated substrate. The surface is very flat. B) SEM micrograph shows that MSCs anchor on biomineralized flagella substrate by filopodia-like extensions.

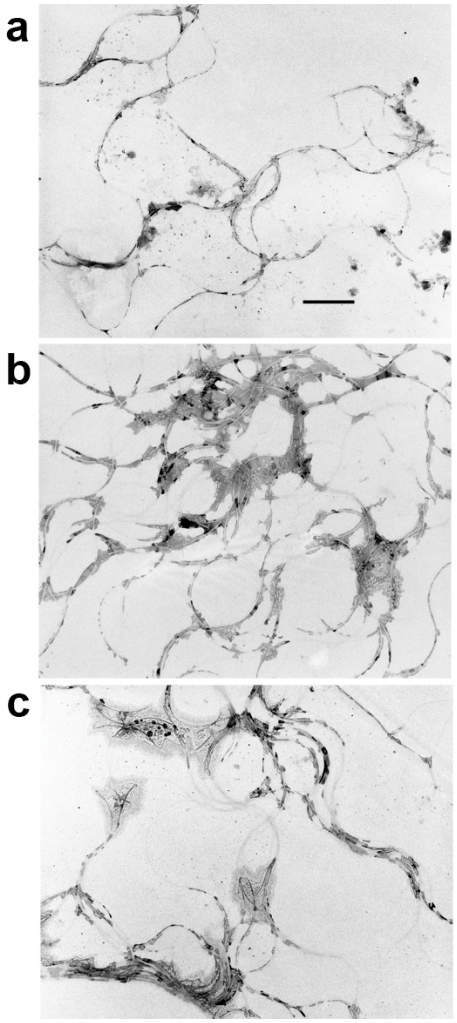

Figure S3. More TEM micrographs of GPP8 flagella mineralized in 4 mM supersaturated HAP precursor solution for 6 days under different flagella concentrations, Related to Figure

2. **a,** Only monodisperse flagella could be observed at a low concentration (~5 μg/ml). The surfaces of flagella were still coated by a layer of inorganic minerals. **b,** At a higher flagella concentration (~15 μg/ml), some bundle-like nanostructures could be observed. **c,** More ribbon-like parallel nanostructures assembled by flagella were formed at a flagella concentration of ~30 μg/ml. It should be noted that these samples were not stained intentionally. The pure flagella were not visible if not stained. Here flagella were visible because they were mineralized.

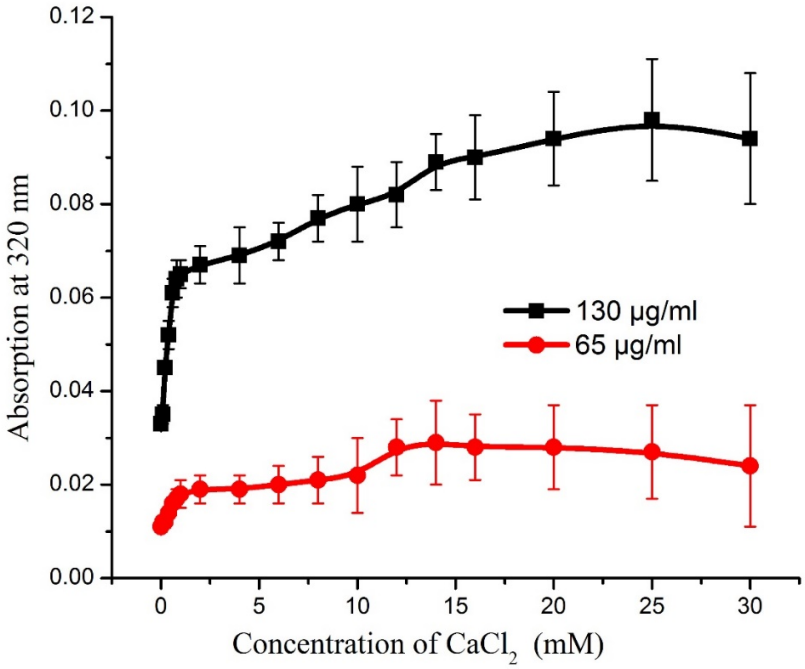

Figure S4. Turbidity measurement (320 nm) of GPP8 flagella solution (65 and 130 μg/ml respectively) after mixed with $CaCl_2$, Related to Figure 2. Initially, with increasing concentration of $CaCl_2$, the absorption of flagella solution was also increased due to the bundle formation. However, after the concentration reached a certain level (~14 mM $CaCl_2$ in 65 μg/ml flagella and ~25 mM $CaCl_2$ in 130 μg/ml flagella), the absorption of flagella solution started to decrease with increasing concentration of $CaCl_2$ due to the depolymerization of flagella.

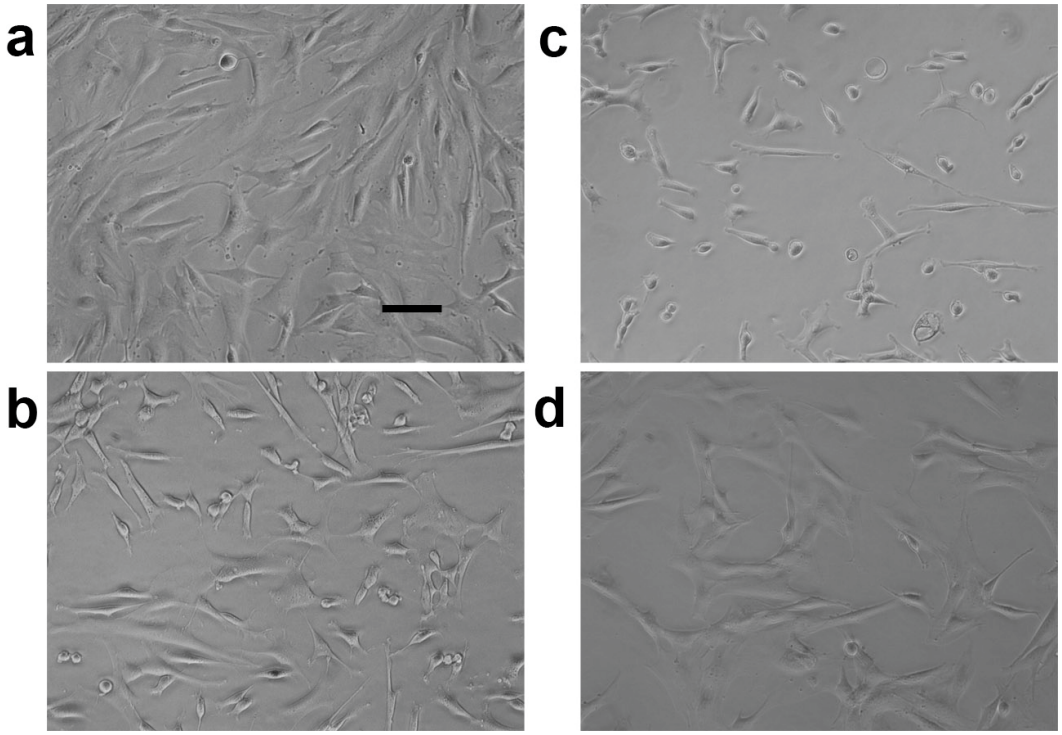

Figure S5. Bright field microscopy of BMSCs on different substrates after 24 h, Related to Figure 3. a, BMSCs on type I collagen. Most cells exhibited a spindle-like morphology and some of the cells were parallel to each other. **b,** BMSCs on GPP8 flagella. The cells had a spindle to polygonal morphology and some of them were stretched at one direction. **c,** BMSCs on the WT flagella. The cells were much less spread and the number of attached cells was less than that on the other substrates. **d,** BMSCs on polylysine (Control). The cells exhibited a well-spread morphology. (Scale bar: 100 μm).

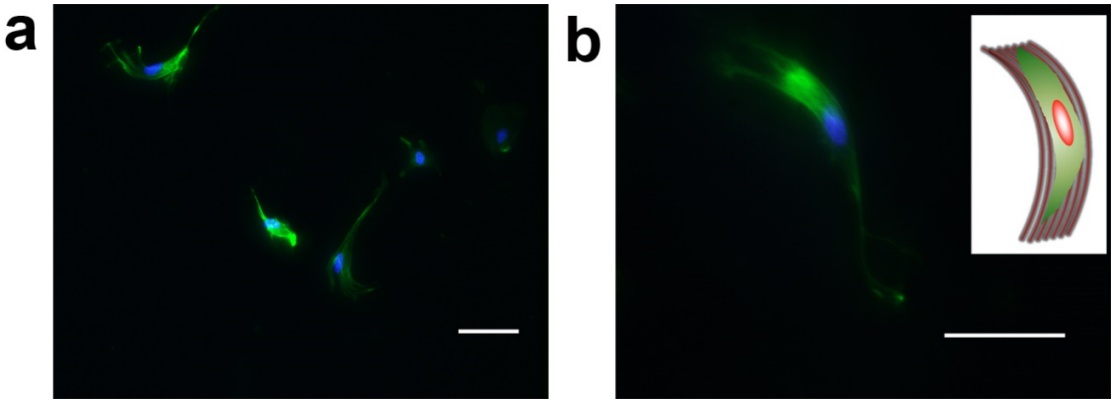

Figure S6. Curly morphologies of BMSCs on the mineralized flagella film after 24 h culture, Related to Figure 3. a, Some cells exhibited curly morphologies on the mineralized GPP8 flagella film. **b,** The BMSCs may attach to the curly portion of flagella bundles and aligned on the substrate by the contact guidance response. Schematic illustration of BMSC adhesion on the flagella bundles (inset) (Scale bar is 100 μm). Cell nuclei were stained by DAPI (blue) and F-actin was stained by FITC-labeled phalloidin (green).

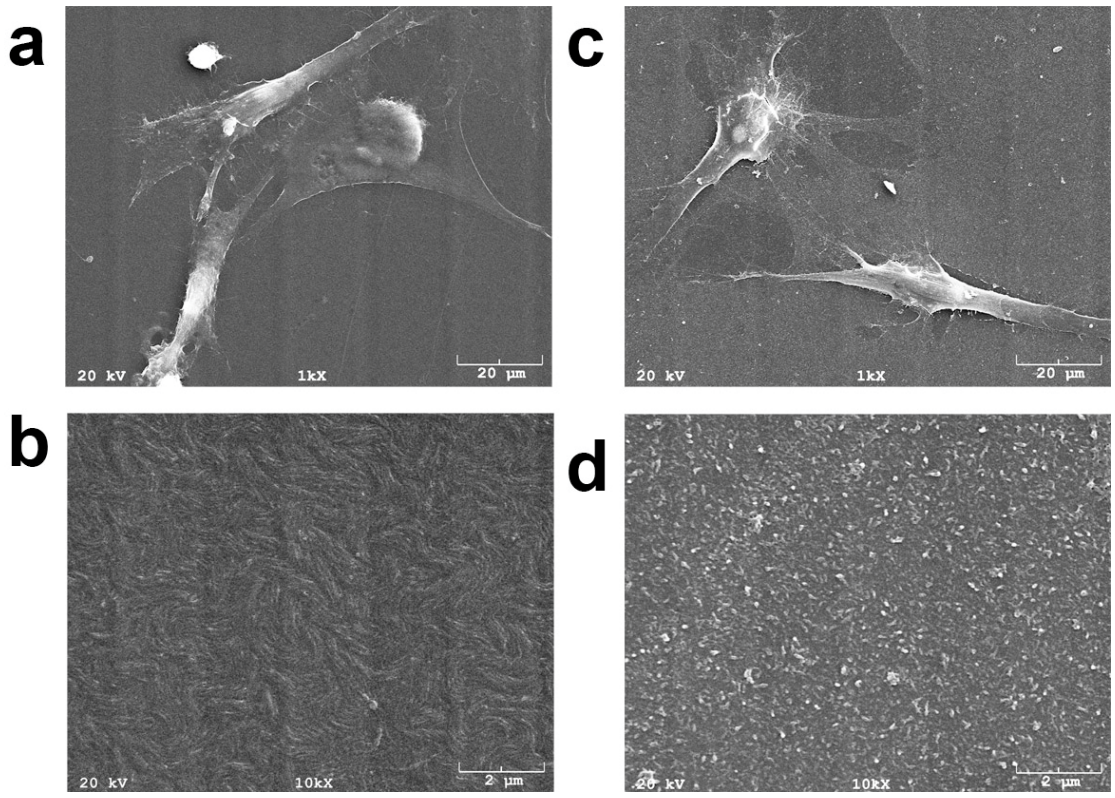

Figure S7 SEM micrographs of BMSCs on collagen and flagella coated films, Related to Figure 3. a, BMSCs on the collagen coated film. The cells were anchored to the substrates through filopodia-like extensions. **b,** At a higher magnification, the collagen-coated film exhibited curly ribbon-like structures that were formed by collagen fibrils. **c,** The cells on the mineralized GPP8 flagella film were less spread and stretched to one direction. **d,** At a higher magnification, mineralized GPP8 flagella coated film showed very rough surfaces due to the nucleation of HAP minerals.

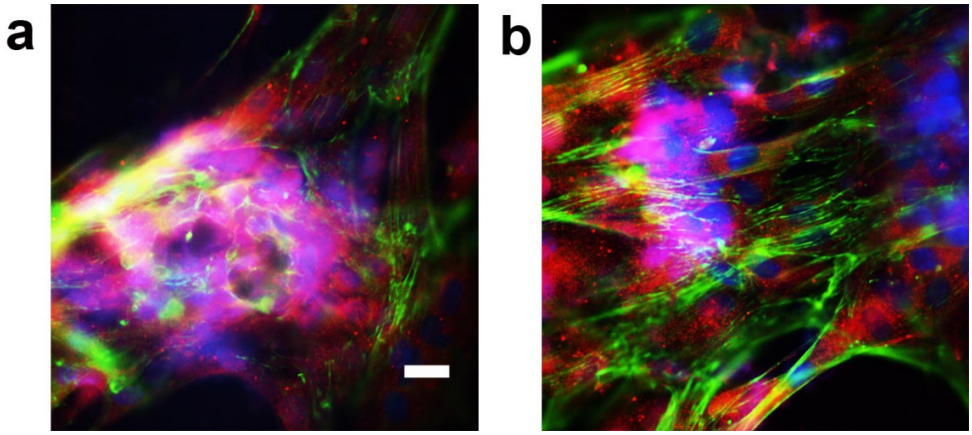

Figure S8 Calcified nodule-like structures of the cells on the GPP8 flagella film after 14 days, Related to Figure 4. a, OPN staining. **b**, OCN staining (Scale bar: 25 μm). The strong expression of OCN and OPN inside the nodule-like structures suggested that the cells are matured toward osteoblast cells. Color code: F-actin (green, stained by FITC-labeled phalloidin); cell nuclei (blue, stained by DAPI); OPN and OCN (red, stained by rhodamine-labeled antibody).